Editors' Suggestion   Featured in Physics

Measurement of the α-Particle Monopole Transition Form Factor Challenges Theory: A Low-Energy Puzzle for Nuclear Forces?

S. Kegel,[1] P. Achenbach,[1] S. Bacca,[1,2] N. Barnea,[3] J. Beričič,[4] D. Bosnar,[5] L. Correa,[6,1] M. O. Distler,[1]
A. Esser,[1] H. Fonvieille,[6] I. Friščić,[5] M. Heilig,[1] P. Herrmann,[1] M. Hoek,[1] P. Klag,[1] T. Kolar,[7,4] W. Leidemann,[8,9]
H. Merkel,[1] M. Mihovilovič,[1,4] J. Müller,[1] U. Müller,[1] G. Orlandini,[8,9] J. Pochodzalla,[1] B. S. Schlimme,[1]
M. Schoth,[1] F. Schulz,[1] C. Sfienti,[1,*] S. Širca,[7,4] R. Spreckels,[1] Y. Stöttinger,[1] M. Thiel,[1] A. Tyukin,[1]
T. Walcher,[1] and A. Weber[1]

[1]*Institut für Kernphysik, Johannes Gutenberg-Universität Mainz, D-55099 Mainz, Germany*
[2]*Helmholtz-Institut Mainz, Johannes Gutenberg-Universität Mainz, D-55099 Mainz, Germany*
[3]*Racah Institute of Physics, Hebrew University, 91904 Jerusalem, Israel*
[4]*Jožef Stefan Institute, SI-1000 Ljubljana, Slovenia*
[5]*Department of Physics, Faculty of Science, University of Zagreb, 10000 Zagreb, Croatia*
[6]*Université Clermont Auvergne, CNRS/IN2P3, LPC, F-63000 Clermont-Ferrand, France*
[7]*Faculty of Mathematics and Physics, University of Ljubljana, SI-1000 Ljubljana, Slovenia*
[8]*Dipartimento di Fisica, Università di Trento, Via Sommarive 14, I-38123 Trento, Italy*
[9]*Instituto Nazionale di Fisica Nucleare, TIFPA, Via Sommarive 14, I-38123 Trento, Italy*

We perform a systematic study of the α-particle excitation from its ground state 0_1^+ to the 0_2^+ resonance. The so-called monopole transition form factor is investigated via an electron scattering experiment in a broad Q^2 range (from 0.5 to 5.0 fm^{-2}). The precision of the new data dramatically supersedes that of older sets of data, each covering only a portion of the Q^2 range. The new data allow the determination of two coefficients in a low-momentum expansion, leading to a new puzzle. By confronting experiment to state-of-the-art theoretical calculations, we observe that modern nuclear forces, including those derived within chiral effective field theory that are well tested on a variety of observables, fail to reproduce the excitation of the α particle.

The rather complex nature of the strong interaction generates a broad range of diverse phenomena in the Universe, which can be experimentally observed and theoretically interpreted. Among the phenomena that are most easily experimentally accessible are those involving strongly interacting matter in the form of atomic nuclei, built from quarks and gluons confined within nucleons. At energies characteristic of nuclear binding, the strength and complexity of quantum chromodynamics (QCD) complicate immensely the understanding of nuclear phenomena in terms of quarks and gluons as fundamental degrees of freedom. Providing a link between QCD with its inherent symmetries and the strong force acting in nuclear systems is a key problem in modern nuclear physics. From the theoretical point of view, a major breakthrough was spurred by the introduction of the concept of effective field theory, which, applied to low-energy QCD, gave rise to the so-called interactions from chiral effective field theory (χEFT) [1–4], where nucleon-nucleon (NN) and three-nucleon (3N) (and more-nucleon) forces arise in a natural and consistent hierarchical scheme. Developments in χEFT, together with advancements in few- and many-body methods, enable controlled calculations of matter at nuclear densities and, recently, even offer the opportunity to extend into the high-density regimes of nuclear matter found in neutron stars [5].

In order to understand exciting phenomena such as neutron star mergers [6], knowledge of the nuclear equation of state is required. The latter is described in terms of a few parameters, such as the symmetry energy, its slope, and the incompressibility [7]. These quantities, ultimately stemming from QCD and recently derived from χEFT using *ab initio* methods [8,9], can be connected to the physics of finite nuclei. For example, the incompressibility K, giving information about the stiffness of nuclear matter against variations in the density, has been traditionally extracted from studies of the isoscalar monopole resonance [10], which is interpreted as a breathing mode.

In this Letter, we study the isoscalar monopole resonance of the α particle in its transition from the ground state 0_1^+ to the first excited state 0_2^+.

The α particle is particularly interesting because it can be addressed as a four-nucleon problem with numerical methods that are accurate even at the subpercent level, leaving any discrepancy with experiment to be blamed on the only input, namely, the assumptions on the used nuclear Hamiltonian, consisting of the choice of nucleons as

effective degrees of freedom and of their relative effective potential.

In particular, the α-particle $0_1^+ \to 0_2^+$ transition calculation based on state-of-the-art χEFT $NN + 3N$ potentials [11] showed a strong disagreement with the existing experimental data (χEFT being up to a factor 2 larger). The existing data [12–14] date back to the early 1970s, with the most recent dataset from 1983. Because of past technical limitations, these measurements suffered from large uncertainties. In addition, unknown normalizations between the different datasets, each covering only part of the Q^2 range of interest, call for new, more precise systematic measurements.

For this purpose, an extensive experimental campaign to measure the ^{4}He monopole transition form factor with high precision was performed at the Mainz Microtron MAMI [15,16]. The measured reaction is $e^- + {}^4\text{He} \to {}^4\text{He}^*(0_2^+) + e^{-\prime}$, where the resonance is excited by Coulomb scattering. The differential cross section of this reaction was measured using the three spectrometer setup of the A1 Collaboration [17].

The continuous-wave electron beam with energies of 450, 690, and 795 MeV was rastered over a cryogenic helium target. The target (see Ref. [16] for details) consisted of cryogenic helium gas encapsulated in an aluminium cell with 250 μm thick walls. The cylindrical target cell has a diameter of 80 mm [18], which results in an areal density of 320 mg/cm² for production data. Permanent pressure and temperature measurements of the target gas allowed a precise (better than 1%) determination of the helium density on the order of $\rho_{^4\text{He}} = 40$ mg/cm³.

The two high-resolution magnetic spectrometers A and B were positioned at various forward scattering angles, covering the Q^2 range from 0.5 to 5.0 fm^{-2}, where the four-momentum transfer Q^2 is given by $Q^2 = q^2 - \omega^2$, with $q = |\vec{q}|$ as the three-momentum transfer and ω as the energy transfer.

The electrons were detected using four layers of vertical drift chambers for particle track reconstruction, two layers of scintillators as the trigger system, and a gas Cherenkov detector for electron-pion separation [19]. The overall relative momentum resolution between 430 and 780 MeV/c was determined to be $\delta \approx 2 \times 10^{-4}$. Because of the large relative momentum acceptances of spectrometer A (20%) and B (15%), both the monopole resonance and the ^{4}He elastic peak could be detected simultaneously. An eventwise separation is possible by calculating the missing mass $m_{\text{miss}} = m_{\text{inv}} - M_{^4\text{He}} = \sqrt{M_{^4\text{He}}^2 + 2M_{^4\text{He}}(E_i - E_f) - Q^2} - M_{^4\text{He}}$, which peaks at zero for elastic scattering, whereas the monopole peak is centered at about 20 MeV. Here, E_i is given by the beam energy, the final electron energy E_f and the four-momentum transfer Q^2 are reconstructed from the detector data.

From the ^{4}He elastic peak and its corresponding form factor [20], the experimental luminosity can be determined precisely. In addition, the width of the elastic peak is used to estimate the experimental resolution needed for precise extraction of the width Γ_0 of the monopole resonance.

In the analysis of the data to obtain the transition form factor, background determination and subtraction is an essential part. Background contributions originate from electron scattering of the aluminium cell walls, the radiative tail of the elastic peak, and the continuum of ^{4}He. A vertex cut could not be used to subtract such background because of the limited vertex resolution and varying angle that would have resulted in a significant reduction of data while introducing additional systematic errors. Instead, dedicated runs were performed for each setup with effectively reduced target gas density ($\rho_{^4\text{He}} \approx 4$ mg/cm³) to determine the background contribution from the aluminium cell, almost exclusively consisting of ^{27}Al. A measurement with a complete empty cell was not performed to avoid thermal stressing of the cell material. With these data, simulations for a complete model of the target cell background were designed and tested, including typical electron scattering processes on ^{27}Al [21]. Phenomenological models for elastic form factors [22] were used to simulate the elastic scattering of ^{27}Al, providing a good agreement between model and data taken with reduced target gas density.

Moreover, the excited states of ^{27}Al listed in Ref. [23] could be observed in the missing mass (m_{miss}) spectrum and were embedded in the simulation as well. An additional background contribution is given by two-body breakup processes from quasielastic electron scattering on ^{27}Al for $m_{\text{miss}} \gtrsim 8$ MeV and thus propagates to the region of the monopole resonance. The breakup continuum of ^{27}Al begins with the proton knockout threshold $E_p = 8.2$ MeV and is dominated by two-body breakup processes. Those processes are described and simulated as off-shell-electron scattering in the framework of De Forest [24]. Furthermore, the form factor parametrization from Ottermann et al. [20] has been used to simulate the additional source of background originating from the ^{4}He elastic peak. Radiative corrections, leading to a modification of the final electron energy to about 25%, were taken into account in all simulations as well [25]. Figure 1 shows data and background simulations for the setup with 450 MeV beam energy at a scattering angle $\vartheta_{\text{scat}} = 20.1°$. After background subtraction, the ^{4}He continuum with the monopole resonance centered at 20.21 MeV between proton and neutron breakup threshold is completely separated, as illustrated in Fig. 2.

To extract the transition form factor from the measured cross sections, an appropriate model parametrization of the unknown resonance peak, including radiative corrections, is required. For such parametrizations, the resonance peak is traditionally considered as a convolution of a Gaussian and a Lorentzian distribution, $G(E, E_0, \sigma_{\text{res}})$
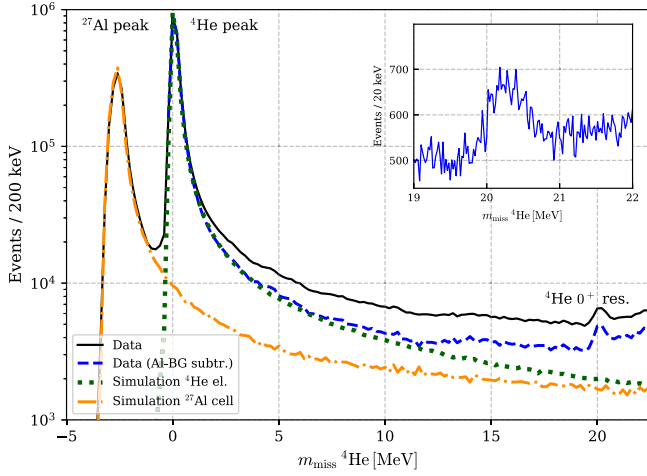
FIG. 1. Missing mass spectrum of ^{4}He. Shown in blue are data for 450 MeV beam energy and a central scattering angle of 20.1° (corresponding to a Q^2 value of 0.59 fm^{-2}.) The data are compared to simulation of the ^{4}He elastic peak (green) and background (BG) contributions from the ^{27}Al target (orange). The contributions from the ^{27}Al elastic peak are located at $m_{\mathrm{miss}} < 0$ due to recoil corrections applied to the scattered electrons. Inset: shows the area of interest, the monopole resonance centered at 20.21 MeV.

and $L(E, E_0, \Gamma_0)$, respectively. While the width of the Gaussian distribution σ_{res} includes experimental resolution effects, the intrinsic width of the resonance is implemented by the full width at half maximum (FWHM) Γ_0 of the Lorentzian distribution. To avoid the complicated
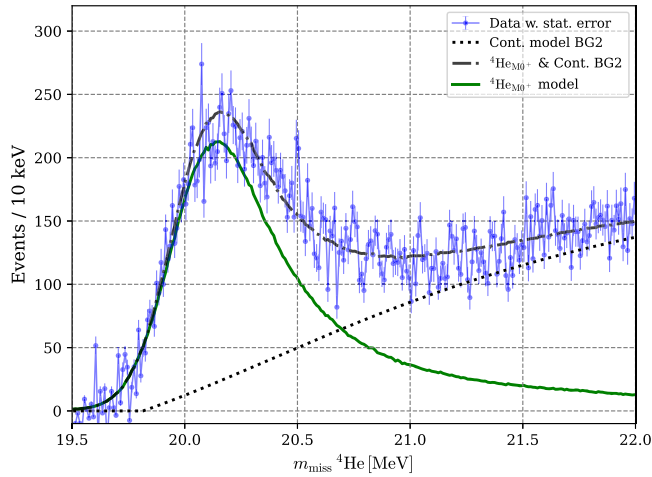

FIG. 2. Typical m_{miss} mass spectrum of the monopole resonance of ^{4}He. Shown with blue points are the data for 690 MeV beam energy with a central scattering angle of 24.0° (corresponding to a Q^2 value of 1.99 fm^{-2}). They are compared to simulation of the monopole resonance (solid green online) and background model BG2 (black dotted line) based on the parametrization of [26]. The dashed line shows the combination of background model and resonance simulation.

convolution integral, the following approximation is used:

$$\sigma_1(E, E_0, \sigma_{\mathrm{res}}, \Gamma_0) \propto \eta L(E, E_0, \Gamma_0) + (1 - \eta) G(E, E_0, \sigma_{\mathrm{res}}). \tag{1}$$

In this ansatz $\eta \in (0, 1)$ is a parameter, constrained by σ_{res} and Γ_0, which regulates the ratio of Gaussian to Lorentzian distribution [27]. In order to quantify more precisely the systematic uncertainties of the described model, a second approach has been used as described in [26,28]. Within this model, the resonance depends on two dimensionless parameters,

$$\mu = \frac{E - E_{\mathrm{thresh}}}{\Gamma_0/2} \quad \text{and} \quad \mu_0 = \frac{E_0 - E_{\mathrm{thresh}}}{\Gamma_0/2}, \tag{2}$$

with $E_0 = 20.21$ MeV being the central value of the resonance and $E_{\mathrm{thresh}} = 19.815$ MeV the continuum proton threshold. The resonance parametrization is taken as

$$\sigma_2(\mu, \mu_0) \propto \frac{(\mu/\mu_0)^{\frac{1}{2}}}{(\mu - \mu_0)^2 + (\mu/\mu_0)}. \tag{3}$$

As a consequence of Eqs. (2) and (3), no resonance events appear below this threshold, as long as resolution and radiative effects are neglected. Resolution effects are implemented in this parametrization by an additional uncertainty of the momentum and angular reconstruction of the spectrometers. This uncertainty is represented by a superposition of two Gaussian distributions with different widths.

To match simulation and data, a complete determination of the previously unknown parameters σ_{res} and Γ_0 is mandatory. The experimental resolution for both parametrizations is determined by the width of the ^{4}He elastic peak, which is broadened by resolution effects and radiative losses. These two contributions are disentangled by Monte Carlo techniques and verified by data. In order to describe the background contribution from the ^{4}He continuum, two model descriptions have been applied to quantify model uncertainties. One model (BG1) describes the continuum under the resonance peak as a linear function, while the second model (BG2) is based on the assumption that the resonance is located on the left tail of a broad giant resonance at 25.95 MeV with $I^P = 1^-$ [29]. For the determination of Γ_0, the simulations of Eqs. (1) and (3), as well as the two background models, were compared to data with Γ_0 as the free parameter to be optimized.

Our results for Γ_0, summarized in Table I, agree within error bars with previous data from Walcher [12,30] and Köbschall _et al._ [13], while they disagree with data from Frosch _et al._ [14], and can be compared to the only theoretical calculation of ^{4}He(e, e'), which resulted in $\Gamma_0 = 180(70)$ keV, using a central NN force [31].

TABLE I. FWHM Γ_0 for the investigated resonance parametrizations σ_1 Eq. (1) and σ_2 Eq. (3) and the two background parametrizations BG1 and BG2.

	BG1 (keV)	BG2 (keV)
σ_1	268 ± 43	285 ± 33
σ_2	262 ± 47	288 ± 39

The transition form factor is obtained from the experimental cross section divided by the normalized Mott cross section,

$$|\mathcal{F}_{\mathrm{M0^+}}(Q^2)|^2 = \left(\frac{d\sigma}{d\Omega}\right)_{\mathrm{Exp}} \Big/ \left(\frac{d\sigma}{d\Omega}\right)_{\mathrm{Mott}}. \quad (4)$$

It is beneficial to take advantage of the simultaneously measured elastic peak of ^{4}He to avoid fluctuations in the data caused by different luminosities and determine the monopole form factor relative to the elastic peak. Both quantities, the elastic peak and the monopole resonance, exhibit a slightly different Q^2 which was accounted for when evaluating the form factor ratio. The value of Q^2 is determined by a binned distribution taking into account the applied data cuts. Those cuts were first restricted to ± 240 keV around both peaks to keep the influence of the continuum background to the form factor ratio small. The relative transition form factor established this way is then in a last iteration step improved by extending the m_{miss} cut from 19.5 to 22 MeV to include large contributions of the monopoles radiative tail. For this purpose, the resonance peak is simulated with parametrization σ_1 and σ_2 and the valid transition form factor ratio and in combination with the backgrounds BG1 and BG2, respectively, optimized to data in order to minimize the χ^2. Within this minimization procedure, the simulation of the monopole resonance peak is allowed to float only by a factor, which is then used to adjust the transition form factor. Further details of the data analysis can be found in the supplemental material [32].

Our final experimental results for the monopole transition form factor are shown in Fig. 3, in comparison to the χEFT calculation from Ref. [11]. A third order basis spline polynomial is used to fit the data. To account for the model uncertainties, the analysis was repeated with all remaining combinations of resonance parametrizations and background models. Analyzing the transition form factor with model BG1 leads to a variation of $\delta_{\mathrm{BG\,model}} = \pm 3.2\%$ around the results obtained by BG2, see Table II. However, a constant shift of the transition form factor to higher or lower values by a different continuum model could not be verified. On the contrary, analyzing the data with σ_1 from (1) leads to an average shift of the transition form factor of $\delta_{\mathrm{res\,model}} = -5.8\%$ and thus to smaller values. These model dependencies were added linearly
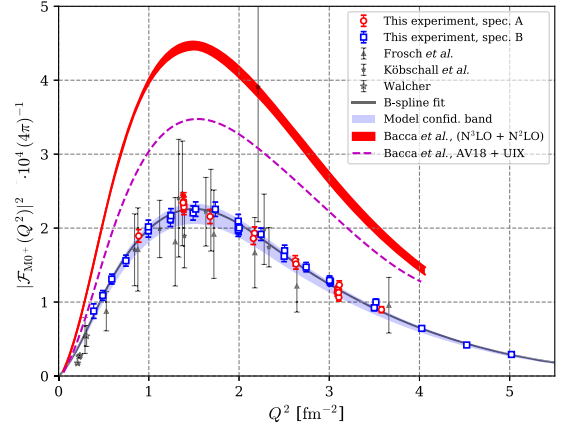

FIG. 3. Monopole transition form factor as a function of Q^2, in comparison to previous data [12–14] and χEFT prediction [11] (see text for details).

to the (blue) model confidence band in Fig. 3, representing the model uncertainty of the data. The contributions to the total systematic uncertainty on the extraction of the transition form factor are summarized in Table II. A conservative error of the elastic form factor of ^{4}He, used to normalize the data, has been estimated as point-to-point uncertainty to 0.5% as given by the authors in [20]. Background subtraction of the elastic tails from ^{4}He, ^{27}Al, and the quasielastic scattering off ^{27}Al contribute to the systematic uncertainty with up to 1%. The FWHM of the monopole resonance Γ_0 influences the transition form factor $|\mathcal{F}_{\mathrm{M0^+}}(Q^2)|^2$ by 4% and contributes the major uncertainty. This uncertainty has been estimated by varying Γ_0 within a realistic error range and observing the effect onto the transition form factor. All systematic errors were added quadratically to the statistical errors. Our results agree with previous data [13,14] albeit having a much higher precision and thereby reinforce the tension with *ab initio* calculations [11], where, for example, the χEFT result is 100% too high at $Q^2 = 1.5$ fm^{-2} with respect to the new data.

Since the low-q^2 part of the transition form factor allows for a direct access to gross features of the 0_2^+ state, we shall focus now on discussing this q^2 range. A $\vec{q} \to 0$ expansion yields [33,34]

TABLE II. Contributions to the systematic uncertainties of the transition form factor and the model dependencies.

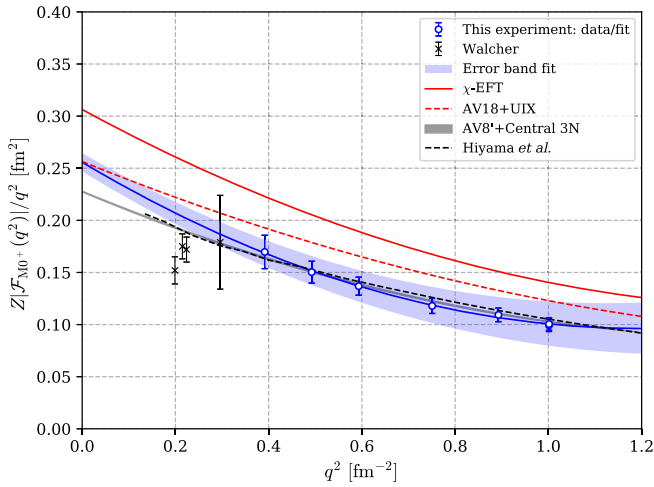| Source	$\Delta|\mathcal{F}_{\mathrm{M0^+}}(Q^2)|^2$ (%)
Background	± 1
^{4}He ground state form factor	± 0.5
$\Delta\Gamma_0$	± 4
Model uncertainties	
BG1-BG2	± 3.2
$\sigma_1 - \sigma_2$	-5.8

FIG. 4. Low-q^2 data for the monopole form factor: theory vs experiment (see text for details).

$$\frac{Z|\mathcal{F}_{\mathrm{M0^+}}(q^2)|}{q^2} = \frac{\langle r^2 \rangle_{\mathrm{tr}}}{6}\left[1 - \frac{q^2}{20}\mathcal{R}^2_{\mathrm{tr}} + \mathcal{O}(q^4)\right] \quad (5)$$

and allows extraction of the monopole transition matrix element $\langle r^2 \rangle_{\mathrm{tr}}$ and the transition radius $\mathcal{R}^2_{\mathrm{tr}} = \langle r^4 \rangle_{\mathrm{tr}}/\langle r^2 \rangle_{\mathrm{tr}}$, which provide information about the spatial structure of the resonant state 0^+_2. We use this formula to extract these quantities both from experimental data and theoretical calculations using a three-parameter fit. For the theory, given that $\mathcal{F}_{\mathrm{M0^+}}$ was calculated on a grid of q every 0.25 fm^{-1} [11], we use four available low-momentum points at $q^2 \leq 1$ fm^{-2}, assigning to each point a 1% numerical uncertainty. The fit values for $\langle r^2 \rangle_{\mathrm{tr}}$ and $\mathcal{R}_{\mathrm{tr}}$ are compatible with what we obtain from a direct calculation using the transition density in coordinate space [35]. For the experiment, we fit the six data points below $q^2 = 1$ fm^{-2} neglecting any recoil and assuming a sharp resonance. A physics boundary condition $\mathcal{F}_{\mathrm{M0^+}}(Q^2 \to 0) = 0$ (which arises from the fact that the inelastic form factor is going to zero for $q^2 \to 0$) was implemented in the spline polynomial fit function of the form factor. The obtained values for $\langle r^2 \rangle_{\mathrm{tr}}$ and $\mathcal{R}_{\mathrm{tr}}$ are reported in Table III with the uncertainties given by the fit, and the corresponding curves based on the mean values of Table III are shown in Fig. 4.

We notice that in the range of $0.2 \leq q^2 \leq 1$ fm^{-2} the simplified potential used by Hiyama *et al.* [36] leads to agreement with the experimental data, while the realistic calculations do not. Because the calculation by Hiyama *et al.* was performed with a distinct few-body method, in this Letter we recalculate it with the same method as in Ref. [11] to infer whether the difference stems from the numerical solver or from the Hamiltonian. In Fig. 4, we show that we (gray solid line) reproduce the result of Ref. [36] (black dashed line). We assign a 1% uncertainty to our calculation by taking the difference from the largest and second largest model-space results. While describing the

TABLE III. Values of $\langle r^2 \rangle_{\mathrm{tr}}$ and $\mathcal{R}_{\mathrm{tr}}$: Experiment vs theory.

	$\langle r^2 \rangle_{\mathrm{tr}}$ (fm^2)	$\mathcal{R}_{\mathrm{tr}}$ (fm)
Experiment	1.53 ± 0.05	4.56 ± 0.15
Theory (AV8'+ central 3N)	1.36 ± 0.01	4.01 ± 0.05
Theory (AV18 + UIX)	1.54 ± 0.01	3.77 ± 0.08
Theory (χEFT)	1.83 ± 0.01	3.97 ± 0.05

data, the AV8'+ central 3N potential is, however, not compatible with the experimental fit value of $\langle r^2 \rangle_{\mathrm{tr}}$, while the realistic AV18 + UIX is. Overall, we see that theory predicts a smaller value of $\mathcal{R}_{\mathrm{tr}}$ than the experimental fit, and the χEFT prediction deviates the most from experiment, even at low momenta. The combination of the new experimental data and calculations prove that there is a puzzle, which is not due to the applied few-body method, but rather to the modeling of the nuclear Hamiltonian. The experimental transition radius is $\approx$10% larger than the calculation with chiral NN-interaction predicts. This might indicate that the hard core of the interaction is too weak, effectively producing a too narrow wave function. Interestingly, another recent investigation [37] shows that the 0^+_2 state in ^{4}He is very sensitive to the particular parametrization of the chiral 3N force.

Further theoretical work is needed to resolve the α-particle monopole puzzle. A systematic experimental verification of future theoretical developments will be opened up by the low-energy electron beam of the new Mainz Energy-recovering Superconducting Accelerator (MESA) under construction at [38], which will operate in the ideal energy regime to test χEFT. Such future generation experiments will allow us to investigate other observables, as well as other light nuclei, leading to an improvement of our current understanding of the nuclear forces.

*sfienti@uni-mainz.de

[1] U. van Kolck, Phys. Rev. C **49**, 2932 (1994).

[2] P. F. Bedaque and U. van Kolck, Annu. Rev. Nucl. Part. Sci. **52**, 339 (2002).

[3] E. Epelbaum, H.-W. Hammer, and Ulf.-G. Meissner, Rev. Mod. Phys. **81,** 1773 (2009).

[4] R. Machleidt and D. Entem, Phys. Rep. **503,** 1 (2011).

[5] C. Drischler, J. Holt, and C. Wellenhofer, Annu. Rev. Nucl. Part. Sci. **71,** 403 (2021), and references therein.

[6] B. P. Abbott et al. (LIGO Scientific and Virgo Collaborations), Phys. Rev. Lett. **119,** 161101 (2017).

[7] A. Steiner, M. Prakash, J. Lattimer, and P. Ellis, Phys. Rep. **411,** 325 (2005).

[8] G. Hagen, A. Ekström, C. Forssén, G. R. Jansen, W. Nazarewicz, T. Papenbrock, K. A. Wendt, S. Bacca, N. Barnea, B. Carlsson, C. Drischler, K. Hebeler, M. Hjorth-Jensen, M. Miorelli, G. Orlandini, A. Schwenk, and J. Simonis, Nat. Phys. **12,** 186 (2016).

[9] B. Hu et al., Nat. Phys. **18,** 1196 (2022).

[10] J. Blaizot, Phys. Rep. **64,** 171 (1980).

[11] S. Bacca, N. Barnea, W. Leidemann, and G. Orlandini, Phys. Rev. Lett. **110,** 042503 (2013).

[12] T. Walcher, Phys. Lett. **31B,** 442 (1970).

[13] G. Köbschall, C. Ottermann, K. Maurer, K. Röhrich, C. Schmitt, and V. Walther, Nucl. Phys. **A405,** 648 (1983).

[14] R. Frosch, R. Rand, H. Crannell, J. McCarthy, L. Suelzle, and M. Yearian, Nucl. Phys. **A110,** 657 (1968).

[15] H. Herminghaus, A. Feder, K. H. Kaiser, W. Manz, and H. V. D. Schmitt, Nucl. Instrum. Methods **138,** 1 (1976).

[16] S. Kegel, Systematic investigation of the ^{4}He monopole, Ph.D. thesis, Johannes Gutenberg-Universität Mainz, 2019.

[17] K. I. Blomqvist et al., Nucl. Instrum. Methods Phys. Res., Sect. A **403,** 263 (1998).

[18] M. Kohl, Elektroproduktion von π^+-Mesonen an ^{3}He und das Studium von Mediumeffekten, Ph.D. thesis, Darmstadt Technical University, 2001.

[19] B. S. Schlimme et al. (A1 and MAGIX Collaborations), Nucl. Instrum. Methods Phys. Res., Sect. A **1013,** 165668 (2021).

[20] C. Ottermann, G. Köbschall, K. Maurer, K. Röhrich, C. Schmitt, and V. Walther, Nucl. Phys. **A436,** 688 (1985).

[21] R. H. Helm, Phys. Rev. **104,** 1466 (1956).

[22] J. Friedrich and N. Voegler, Nucl. Phys. **A373,** 192 (1982).

[23] M. S. Basunia, Nucl. Data Sheets **112,** 1875 (2011).

[24] T. De Forest, Nucl. Phys. **A392,** 232 (1983).

[25] M. Vanderhaeghen, J. M. Friedrich, D. Lhuillier, D. Marchand, L. Van Hoorebeke, and J. Van de Wiele, Phys. Rev. C **62,** 025501 (2000).

[26] J. D. Jackson, Nuovo Cimento **34,** 1644 (1964).

[27] Y. Liu, J. Lin, G. Huang, Y. Guo, and C. Duan, J. Opt. Soc. Am. B **18,** 666 (2001).

[28] S. Margulies and J. J. Phelan, Il Nuovo Cimento A (1965–1970) **58,** 804 (1968).

[29] D. R. Tilley, H. R. Weller, and G. M. Hale, Nucl. Phys. **A541,** 1 (1992).

[30] T. Walcher, Z. Phys. **237,** 368 (1970).

[31] W. Leidemann, Phys. Rev. C **91,** 054001 (2015).

[32] See Supplemental Material at http://link.aps.org/supplemental/10.1103/PhysRevLett.130.152502 for further analysis details.

[33] H. Theissen, Spectroscopy of Light Nuclei by Low Energy (<70 MeV) Inelastic Electron Scattering (Springer, Berlin, Heidelberg, 1972), pp. 1–57.

[34] M. Chernykh, Electron scattering on ^{12}C, the structure of the Hoyle state and a neutron ball for $(e, e'n)$ experiments at the S-DALINAC, Ph.D. thesis, Technische Universität Darmstadt, 2008.

[35] S. Bacca, N. Barnea, W. Leidemann, and G. Orlandini, Phys. Rev. C **91,** 024303 (2015).

[36] E. Hiyama, B. F. Gibson, and M. Kamimura, Phys. Rev. C **70,** 031001(R) (2004).

[37] M. Viviani, L. Girlanda, A. Kievsky, and L. E. Marcucci, Phys. Rev. C **102,** 034007 (2020).

[38] N. Berger, A. Denig, F. Maas, and C. Sfienti, Nucl. Phys. News **31,** 3 (2021).